AIAA JOURNAL
Vol. 43, No. 3, March 2005

Reduced-Order-Model Approach for Aeroelastic Analysis Involving Aerodynamic and Structural Nonlinearities

Sorin Munteanu,* John Rajadas,† Changho Nam,‡ and Aditi Chattopadhyay§
Arizona State University, Tempe, Arizona 85225

A reduced-order model (ROM) for solving an aeroelasticity problem including structural and aerodynamic nonlinearities is introduced. The aerodynamic system is identified using a Volterra-based ROM. The appropriate procedures needed for the identification of the aerodynamic linearized kernel are presented, and a procedure to identify the first- and second-order Volterra kernels and a linearized ROM kernel from aerodynamic step response is detailed. A coupled framework for addressing the nonlinear aeroelasticity problem using a typical wing section model is introduced for the validation of the procedure. Nonlinear unsteady aerodynamic forces in both subsonic and transonic regimes are evaluated using a conventional approach using the CFL3D (version 6.1) code capable of integrating Navier–Stokes and the structural equations. The computational-fluid-dynamics (CFD) solver is used to compute the aerodynamic response to step or impulse inputs. Aerodynamic responses to arbitrary inputs are predicted using ROM kernels. The Gaussian pulse response obtained using ROM was validated by comparison with the response obtained from CFD solver. Aeroelastic analysis was conducted using the ROM with aerodynamic and structural nonlinearities. The results show that the reduced-order model can estimate accurately flutter speed as well as the limit-cycle oscillations (LCO). Also the ROM approach is found to be computationally efficient.

I. Introduction

AIRCRAFT structures suffer aeroelastic problems as a result of strong interactions between the flexible aircraft structures and the surrounding flow.[1] These interactions are nonlinear and need analysis tools that are capable of addressing such nonlinear phenomena for proper understanding. Development of aeroelastic analyses for nonlinear fluid dynamic phenomena is still an evolving field.[2,3] Closed-form solutions are available only for aeroelastic problems when flow characteristics are linear. Beckert[4] used a computational-fluid-dynamics (CFD) code in conjunction with a computational-structural-dynamics (CSD) code to predict aeroelastic deformations under specified flight conditions. Chattopadhyay et al.[5,6] integrated CFD and CSD codes for the analysis and design optimization of high-speed civil transport and turbomachinery blades. The coupling of high-fidelity CFD and CSD tools to address aeroelastic problems has received considerable interest in the recent years.[7,8] Uncoupled and coupled methods for solving these nonlinear problems exist.

Two main formulations have emerged in the efforts to address nonlinear aeroelastic problems. They are the monolithic and the coupled field formulations.[4] The monolithic formulation involves strongly coupled single-domain solutions using the CFD and CSD equations simultaneously. This requires the reformulation of the equations for each discipline. Recently, there have been renewed attempts to solve both the fluids and structures problems in a single computational domain. However, these efforts have been limited to simple two-dimensional problems and have not proven to be better than the loosely coupled approach.[8] In the coupled field formulation, the coupled problem is solved using existing well-established numerical solvers. The interaction between the fluid and structural phenomena is limited to the exchange of surface loads and surface deformation information.[3,7]

Although the area of nonlinear aeroelasticity has received significant attention from the research community, most of the methods developed address only aerodynamic nonlinearities.[9,10] A CFD time-marching analysis using the CFL3D solver[11] was conducted to investigate the transonic limit-cycle oscillation (LCO) of a typical section model.[12] The development of efficient nonlinear structural analysis procedures is a critical element in the integrated CFD/CSD system. In most existing studies, the structural analysis has been linearized to simplify the complexity of the integrated system. The presence of the structural nonlinearities in an aeroelastic system makes the response associated with the LCO and chaotic motion nonlinear. Ko et al.[13] derived an adaptive nonlinear feedback control methodology for a structurally nonlinear typical wing section model. For this model, which includes a pitch-hardening spring, the linear control methodologies proved not to be consistently stable in the presence of LCO, and an adaptive nonlinear feedback control methodology is used. The free play and the geometric structural nonlinearities are two main causes of structural nonlinearities.[14] Flutter-induced LCOs can be experienced as a result of control surface free play. Ignoring the nonlinear behavior of the structure usually leads to overestimation of the structural stiffness by underpredicting the structural deformation, underestimation of the ultimate strength and load-carrying capacity of the structure, and misspredictions of the dynamic response. All of these can lead to inaccurate predictions of aeroelastic response.

Incorporation of a CFD code into a fluid-structure interface solver will typically result in high computational cost. The efficiency and utility of superposition of scaled and shifted fundamental responses have been recognized as a powerful tool for improving the computational efficiency of the methods for modeling the unsteady aerodynamic responses. Classical models of airfoils in incompressible flows include Wagner's function or Theodorsen's function. For the case where geometry or flow-induced nonlinearities are significant in the aerodynamic response, time integration of the nonlinear equations is necessary (as in CFD codes) for aeroelastic analysis. One approach to this problem is the development of CFD-based reduced-order models (ROMs), which capture the essence of the dynamical system under investigation while reducing the complexity of the computational model.[15] Thomas et al. used proper orthogonal decomposition (POD) to compute a linear basis from a series of flow solutions in order to reduce the computational cost

Received 18 May 2004; revision received 4 October 2004; accepted for publication 5 October 2004.

*Graduate Student, Mechanical and Aerospace Engineering Department. Student Member AIAA.
†ASC Professor, Mechanical and Manufacturing Engineering Technology Department, ASU East. Associate Fellow AIAA.
‡ASC Professor, Mechanical and Manufacturing Engineering Technology Department, ASU East. Senior Member AIAA.
§Professor, Mechanical and Aerospace Engineering Department. Associate Fellow AIAA.

of integrating Euler equations for arbitrary geometry. The development of a frequency-domain form of the POD technique using flow solutions at a number of discrete frequencies for pitching and plunging airfoil motions is presented in Ref. 16. Using ROMs based on the Volterra theory is one of several options currently available.[17] These ROMs are based on the creation of unsteady impulse or step responses. The pulse or step responses are used in a convolution scheme to provide the response of the system to arbitrary inputs. The Volterra-based ROM approach has been applied extensively for solving fluid-structure interaction phenomena using nonlinear CFD solvers and linear structural dynamic solvers including a modal analysis.[18] The step or pulse response was identified for each mode of the aeroelastic system using an aeroelastic CFD code. Silva[18] used the pulse response to identify the first- and second-order Volterra kernels and predict the aerodynamic response to an arbitrary input. Silva and Raveh[19] used convolution of the step response with the derivative of the displacement to predict the aerodynamic forces. Although the step-response identification involves reduced numerical complexities caused by lower gradients, the prediction of nonlinear aerodynamic response cannot be identified using the Duhamel integral procedure because this procedure is based on a superposition integral valid only for linear systems and can provide reasonable linearized predictions only for weakly nonlinear systems. Silva's approach[17] provides insightful information about the aerodynamic nonlinearities via the second-order Volterra kernels. These approaches do not fully address the nonlinear interactions because the aeroelastic analysis did not include structural nonlinear phenomena. A treatment of linearized, CFD-based pulse responses as Markov parameters for implementing an identification/realization system algorithm was used in Refs. 20 and 21.

The focus of the present paper is the application of the ROM methodology for the aeroelastic analysis of wing structures with structural nonlinearities. A primary task was to develop an interface model for the fluid/structure-interaction problem for a coupled nonlinear aeroelastic model.[22] A computational framework based on ROM kernels is developed. A quasi-linear formulation of nonlinear mode shapes is developed in order to address the structural nonlinearities. For defining the nonlinear transient mode shapes, it is assumed that for a small time step, space variables can be separated and the motion can be expressed in terms of a finite number of modes. The goal is to compute the unsteady aeroelastic responses of the nonlinear structural system coupled with nonlinear aerodynamics. For the ROM approach, the unsteady aerodynamic response is identified using the CFD solver, CLF3D version 6.1. A procedure for identifying and building the first- and second-order ROM kernels from the aerodynamic step or impulse response is developed. Aeroelastic analysis is conducted, and the results are compared with those obtained using the conventional analysis approach.

II. Mathematical Formulation

A. Aeroelastic Analysis

Two different approaches are used to integrate the aeroelastic equations of motion in the work described here. In the conventional approach, the aeroelastic module in the CFL3D solver is used. In the ROM-based approach, CFL3D is used to obtain aerodynamic responses caused by impulse or step inputs and then to generate the ROM kernels. The ROM kernels are then convolved with the arbitrary inputs to predict the aerodynamic response.

There are some differences between the two approaches. CFL3D integrates the aeroelastic equation for the flow computation (Navier–Stokes equations) and structural responses at each time step. The ROM approach uses two steps: a compilation time step where the solver "learns" the aerodynamic response of the flow caused by a pulse or step input and a run-time step where the aerodynamic response is convolved to integrate the aeroelastic equation of motion.

Another difference between the two approaches is related to the grid-deformation algorithm. In the conventional CFD approach, the grid has to be deformed in accordance with the wing deformations at each time step increasing computational cost. In the ROM approach, the grid-deformation algorithm has to be used only twice for each mode when building the aerodynamic response for each structural mode. Thus, the number of grid deformations in the CFD approach is proportional to the number of iterations used in transient computations, whereas in the ROM approach the number of grid deformations is proportional to the number of structural modes.

Because the ROM approach uses just the modal shapes to decompose the aerodynamic response, results of previous runs can be used for structures using the initial modal shapes, which also results in computational efficiency. The ROM approach is based on the assumption that 1) the aerodynamic pulse or step response is not a function of dynamic pressure or Reynolds number and 2) the aerodynamic response is nonlinear but the first-order kernel extracted is linearized, which might be restrictive.

B. CFD-Based Unsteady Aerodynamics

1. Nonlinear Structural Analysis

The structural nonlinearities are addressed using a piecewise linear approach over each time step. The z-direction displacements of the wing over a time step are expressed in the modal coordinates as

$$z(x, y, t_{n+1}) = z(x, y, t_n) + \sum \gamma_{i,n}(t)\, h_{i,n}(x, y) \tag{1}$$

where h_i is the mode shape and γ_i is the generalized modal coordinate. The equations of motion can be obtained from Lagrange's equation as

$$\sum_j \ddot{\gamma}_j \iint_S m h_i h_j \,\mathrm{d}S + \iint_S F(x, y, z_n) h_i \,\mathrm{d}S + \sum_j \gamma_j \iint_S \sigma h_i h_j \,\mathrm{d}S = Q_i \tag{2}$$

where $\sigma(x,y)$ represents the effective stiffness of the wing elastic restoring force, F is the strain force, and m is the mass per unit area. The second term constitutes a nonlinear correction force, which is equal to the projection of the initial restoring elastic force on the ith mode shape. The generalized aerodynamic force Q_i is expressed as

$$Q_i = \frac{\rho U^2}{2} c^2 \iint_S h_i \frac{\Delta p}{c^2 \rho U^2/2} \,\mathrm{d}S \tag{3}$$

where c is the chord, ρ is the density, U is the freestream speed, Δp is the pressure variation, and $h_i(x, y)$ are the mode shapes. A correction force caused by the strain energy has to be added in the equation at the beginning of each time step. This correction force is as a result of the geometric nonlinearities. The mode shapes h_i are functions of time because of the changes in the effective stiffness. The initial condition for each time step has to be computed using the values of z at the previous time step and the continuity of the displacement at each time step. Then, the aeroelastic equation can be written as

$$M_n \ddot{\gamma}_n + K_n \gamma_n = Q - \iint_S F(x, y, z) h \,\mathrm{d}S \tag{4}$$

where M_n is the generalized mass matrix, K_n is the stiffness matrix, and Q is the generalized aerodynamic force vector. By defining $q_{i,n}$ as

$$q_{i,n}(t) = q_{0,i,n}(t_n) + \gamma_{i,n}(t) \tag{5}$$

where $q_{0,i,n}(t_n)$ is the modal coefficient at the previous time step, the equations of motion at the nth step are written as

$$M_n \ddot{q}_n + K_n q_n = Q_{\mathrm{nl}} \tag{6}$$

where

$$Q_{\mathrm{nl},i} = Q_i - \iint_S F(x, y, z) h_{i,n}(x, y) \,\mathrm{d}S + \sum_{j=1}^{n} K_{i,j,n} q_{0,j,n} \tag{7}$$

Equations (6) and (7) are the quasi-linear equations of motion and the initial conditions for the time domain $[t_n, t_{n+1}]$. After incorporating the nonlinear corrections in mass, stiffness, and force, the aeroelastic equation can be expressed in first-order state-space form[23] as

$$\dot{x}_i = A_i x_i + B_i u_i \tag{8}$$

The state vector is $x_i = \lfloor q_i \;\; \dot{q}_i \rfloor^T$. The general solution of the state equation can be written as

$$x_i(t) = \Phi_i(t)x_i(0) + \int_0^t e^{A_i(t-\tau)} B_i u_i(\tau)\,\mathrm{d}\tau \tag{9}$$

Numerically, the solution is advanced from any time step n to next step $n+1$ by

$$x_i[t_{n+1}] = \Phi_i(\Delta t)x_i[t_n] + \int_0^{\Delta t} \Phi_i(\Delta t - \tau)Bu_i(\tau)\,\mathrm{d}\tau \tag{10}$$

where Δt is the step size. After computing the flowfield, the estimation of u_i over the time step can be refined, and the algorithm can be repeated until convergence is reached. A complete description of the technique is presented in Ref. 22.

2. Conventional Aeroelastic Approach

Three sets of calculations are carried out in the conventional approach (using CFL3D). The first is the integration of the Navier–Stokes equations for the steady flow and then the updating of the flow at each time step. The second set involves the grid-deformation process, and the third one is the vibration equation solver. During the transient computations, all three calculations are carried out at each time step. The grid used in this approach is the CFD grid used for flow computations. At each time step, the initial grid is deformed by adding the modal deformations using the generalized coordinates and the mode shapes to obtain the new surface grid. This is then used as the input to the grid deformation solver to compute the full CFD grid.

The equations of motion are given by

$$M_i\ddot{q}_i + C_i\dot{q}_i + K_i q_i = \iint \Delta p(q_1, ..q_n, x, y)h_i(x, y)\,\mathrm{d}S - \iint_S F(x, y, z)h_i(x, y)\,\mathrm{d}S + K_i q_{0,i} \tag{11}$$

where M_i, C_i, and K_i are the diagonalized mass, damping, and stiffness matrices, respectively. Solution of the equation involves the use of subiterations for convergence. In the conventional approach (CFD), every subiteration implies the integration of the Navier–Stokes equations, leading to high computational cost. The use of a reduced-order model helps to reduce the estimation of the new generalized forces to a simple vector multiplication, thus resulting in computational efficiency.

3. ROM Approach

Volterra theory is a generalization of the convolution integral approach often applied to linear, time-invariant systems. The theory states that any time-invariant, nonlinear system can be modeled as an infinite sum of multidimensional convolution integrals of increasing order. This is represented symbolically by the series of integrals (Volterra series) as

$$y(t) = h_0 + \int_0^\infty h_1(\tau_1)u(t-\tau_1)\,\mathrm{d}\tau_1 + \int_0^\infty\int_0^\infty h_2(\tau_1, \tau_2)u(t-\tau_1)u(t-\tau_2)\,\mathrm{d}\tau_1\,\mathrm{d}\tau_2 + \cdots \tag{12}$$

Here, $u(t)$ represents the system input while $y(t)$ represents the system response. Each of the convolution integrals contains a kernel, which represents the behavior of the system. Knowledge of these kernels allows the prediction of a system's response to an arbitrary input. The first-order term represents the mean of the system response. The weakly nonlinear system is usually well represented by the first two or three terms of a Volterra series. All higher-order kernels (higher than second order) are generally negligible in the system representation. Originally, the method of Volterra series and kernel identification was developed to address the nonlinear behavior in electrical circuits. In the aerospace field, the fundamental contributions were from Silva,[9] who has shown that the method is also applicable to aeroelastic systems. The nonlinear Navier–Stokes equations can be considered weakly nonlinear and can be accurately represented by a truncated second-order Volterra series. Linear response models have often been assumed sufficient for the representation of nonlinear aerodynamic systems when excited by small perturbations. This assumption is based on the fact that highly nonlinear phenomena have a negligible impact on the net effect of various responses under conditions of small perturbation excitations. Time is discretized with a set of equal time steps. Discrete time increments are indexed from 0 (time 0) to n (time t), and the evaluation of y at time n, $y(n)$ is given by

$$y(n) = h_0 + \sum_{i=1}^{N} h_1(n-i+1)u(i) + \sum_{i=1}^{N}\sum_{j=1}^{N} h_2(n-i+1, n-j+1)u(i)u(j) \tag{13}$$

Silva[9] developed a procedure to identify the first- and second-order kernels by applying appropriate impulse inputs to the aerodynamic system. The first two kernels are

$$h_1(t) = 2y_0(t) - \tfrac{1}{2}y_2(t) \tag{14}$$

$$h_2(t, t+T) = \tfrac{1}{2}[y_1(t) - y_0(t) - y_0(t+T)] \tag{15}$$

where $y_0(t)$ is the response of the system to a Dirac delta function $u_0(t) = \delta(t)$, $y_1(t)$ is the response of the system to a sum of two Dirac delta functions $u_1(t) = \delta(t) + \delta(t+T)$, and $y_2(t)$ is the response of the system to $u_2(t) = 2\delta(t)$.

Silva and Raveh[19] assumed that the response could be evaluated with only the first term in Volterra kernel. The response of the system to an arbitrary input is computed by the convolution of step response $s(n)$ with the derivative of input signal $u(n)$, according to Duhamel's integral, as

$$y(n) = u(0)s(n) + \sum_{i=1}^{n} s(n-k)[u(k) - u(k-1)] = u(0)s(n) + \sum_{i=1}^{n} s(n-k)\dot{u}(k)\Delta t \tag{16}$$

In the present work, the step excitation approach was used for kernel identification because of the instability of the aerodynamic response when using impulse excitation. The response is postprocessed to obtain the ROM kernels. An example of the kernel identification procedure based on the first three terms of ROM (h_0, h_1, and h_2) is described next.

The first kernel h_0 is the steady-state response of the system when no input is applied, and it can be subtracted from the system response. Hence, one can assume $h_0 = 0$ without loss of generality. Another assumption of this derivation is that the response of the system is influenced only by the last n iterations ($n = T/\Delta t$, where T is the time after which the system "forgets" the old inputs). The procedure to determine T is to excite the system fully and then identify the moment when the effect of the old inputs disappears. Another way is to excite the system with a step impulse and wait until the response converges to a steady state. The impulse response contains only the diagonal terms of the second-order kernel when the input is applied simultaneously [Eq. (17)], whereas the step response contains all of the second-order kernel terms.

$$h_2(n-i+1, n-j+1)u_k(i)u_k(j) = 0$$

$$\text{for} \qquad i \neq 1, \qquad j \neq 1 \tag{17}$$

Because the first-order kernel defined the length of the kernels, estimation of n should provide similar results for both step and impulse inputs:

$$y_k(n) = \sum_{i=1}^{n} h_1(n-i+1)u_k(i) + \sum_{i=1}^{n}\sum_{j=1}^{n} h_2(n-i+1, n-j+1)u_k(i)u_k(j) \tag{18}$$

The goal of the ROM is to predict, by using convolution of ROM kernels, the response of the system for an arbitrary input. For linear problems, identification of the first kernel h_1 is sufficient to identify the system response. Because Navier–Stokes equations can be considered to be weakly nonlinear, the system response can be accurately predicted by using only a first-order ROM kernel that includes the linearized nonlinear effect. The approach to the identification of the kernel is to excite the system with a set of inputs u_k (using the CFD solver) and generate the responses y_k (k is the index of excitation vector). Assuming weak nonlinearity, h_1 and h_2 can accurately predict the response for any input u_k. One can write n linear equations for the $n(n+1)$ unknowns. Assuming symmetry in h_2, the number of unknowns can be reduced to $n(n+3)/2$ by

$$h_2(n-i+1, n-j+1) = h_2(n-j+1, n-i+1) \tag{19}$$

That is, in order to solve the ROM kernel identification problem $n(n+3)/2$ linear equations should be generated. This means that $(n+3)/2$ different cases should be considered to generate the coefficients for a linear system with $n(n+3)/2$ unknowns.

The number of unknowns can be reduced further. The length of the second-order kernel can be considerably smaller than the square of the length of the first-order kernel. To minimize the time needed for generating the equations, the following formulation is used:

$$y_k(n) = \sum_{i=n-n_1+1}^{n} h_1(n-i+1)u_k(i) + \sum_{i=n-n_2+1}^{n}\sum_{j=n-n_2+1}^{n} \times h_2(n-i+1, n-j+1)u_k(i)u_k(j) \tag{20}$$

where n_1 is the length of the first-order kernel and n_2 is the length of the second-order kernel. Now the number of unknowns is $n_1 + n_2(n_2+1)/2$. Although it is easy to find the maximum of the kernel lengths, there is no easy way to estimate the length of each kernel after recording the system response once. Analysis of the problem suggests that the first-order kernel length is higher than the square root of second-order kernel. So, measuring the time after the effect of the excitation on the system disappears gives an accurate measure for the length of first-order ROM kernel.

A procedure to generate the minimum set of computations needed to obtain a linear system of equations for the components of ROM kernels is outlined next. Each equation will be of the form

$$\boldsymbol{y}_k(n) = \sum_{i=n-n_1+1}^{n} h_1(n-i+1)u_k(i) + \sum_{i=n-n_2+1}^{n}\sum_{j=n-n_2+1}^{n} \times h_2(n-i+1, n-j+1)u_k(i)u_k(j) \tag{21}$$

where k is the case index and the vector $\boldsymbol{y}_k$ is the response of the system caused by excitation u_k. The system of equations can be written in matrix notation as

$$A_{MxN}\boldsymbol{x}_N = b_N \tag{22}$$

where $N = n_1 + n_2(n_2+1)/2$. The index M is the number of excitations applied, N is the number of unknowns, $\boldsymbol{x}$ is the vector containing the ROM kernels unknowns and b_N is the free term and contains the responses of the system.

The coefficients of the kernels parameters are of the form $u_k(i)$ and$u_k(i)u_k(j)$. The matrix A is very large, and there is no symmetry for arbitrary inputs. Certain special types of inputs can generate easy to handle coefficient matrices. Silva's[9] strategy on generating the matrix A was to choose each input as a sum of one or two Dirac delta functions. The matrix A generated by those inputs is a sparse matrix that contains, after nondimensionalization, only 0s, 1s, and 2s, which makes the Gaussian-elimination-like procedures exact. Even though the impulse excitation technique is accurate, it is very difficult to implement in the CFD code. To obtain good results, large amplitudes for the impulse have to be applied, and the CFD code might not be able to handle them.

Silva and Raveh[19] mentioned that the step input approach is more robust than the pulse response, while being computationally expensive. In this approach, all of the excitations of the systems will be of amplitude either $\bar{u}_0$ or $2\bar{u}_0$. After a simple nondimensionalization process, the matrix A will contain only 1s, 2s, and 4s, which will make all of the Gaussian-elimination-like operations exact even though the matrix is fully loaded. This approach (1-2-4 strategy), although computationally more expensive than the impulse input approach (0-1-2 strategy),[9] provides a way to generate the equations for solvers that are robust to strong step excitations but can became unstable to strong impulse excitations. The goal is to identify the first-order ROM kernel by applying a step input until the system response reaches steady state and then compute the length of the first-order kernel. The response recorded will contain all of the terms of the second-order kernel. Because the number of unknowns will be higher than the number of equations, additional excitations will be needed to identify the kernels. Only one excitation is needed to eliminate the nonlinear components and to obtain a set of $2n_1$ linear independent equations and $2n_1$ unknowns (all of which are components of first-order ROM kernel). Once the first-order kernel is identified, the linear component of the response can be computed and removed from the already generated response. At this step, the first-order ROM kernel, at least one response of the system to step input that fully excited the second-order kernel, and the nonlinear component of that response have been computed. The number of iterations after which the nonlinear component of the response converges is the length of second-order kernel.

III. ROM Kernel Identification

A. First-Order Kernel Identification

Two step inputs ($k = 1, 2$) are applied for first-order kernel identification. These two vectors will generate the system of equations needed to obtain the linear kernel. Superscript l is used to identify the excitation and response corresponding to the linear kernel here:

$$u_k^l(i) = k\bar{u}_0 \qquad \text{for} \qquad i = 1, 2, \ldots n_1, \qquad k = 1, 2 \tag{23}$$

Although the length of the first-order kernel n_1 is not clearly identified at the beginning of the computation, once the response reaches a steady state n_1 will be the number of iterations. The response of the system to first step input is

$$y_k^l(n) = k\bar{u}_0 \sum_{i=1}^{n} h_1(n-i+1) + k^2\bar{u}_0^2 \sum_{i=1}^{n}\sum_{j=1}^{n} h_2(n-i+1, n-j+1)$$

$$n = 1, 2, \ldots n_1, \qquad k = 1, 2 \tag{24}$$

Simple manipulation of these equations leads to the solution for one term of the second-order kernel and all terms of first-order

kernel:

$$h_2(1,1) = \left[y_1^l(1) - \bar{u}_0 h_1(1)\right] \Big/ \bar{u}_0^2 = \left[y_2^l(1) - 2y_1^l(1)\right] \Big/ \left(2\bar{u}_0^2\right) \tag{25}$$

$$h_1(n) = \left\{4\left[y_1^l(n) - y_1^l(n-1)\right] - \left[y_2^l(n) - y_2^l(n-i)\right]\right\} \Big/ (2\bar{u}_0) \qquad i = 1, 2 \cdots n_1$$

$$y_1^l(0) = 0, \qquad y_2^l(0) = 0 \tag{26}$$

B. Second-Order Kernel Identification

For arbitrary inputs u_k, the nonlinear component of the response P_k can be defined as

$$P_k(n) = y_k(n) - \sum_{i=1}^{n} h_1(n-i+1)u_k(i) \tag{27}$$

P_k can be computed for any arbitrary input u_k, provided that the linear kernel h_1 was identified and the input u_k and outputy_k are known using Eq. (27). Once the first-order kernel is known, the system of equations for h_2 is simplified and becomes a system of linear equations for the second-order kernel:

$$\sum_{i=1}^{n}\sum_{j=1}^{n} \boldsymbol{h}_2(n-i+1, n-j+1)u_k(i)u_k(j) = P_k(n) \tag{28}$$

An induction method is used to solve the equation for $h_2(i, j)$ (28), by solving step by step the equations for the unknown vector $\boldsymbol{h}_2(n, i)\, i = 1 \cdots n$. For $n = 1$, the unknown vector is $\boldsymbol{h}_2(1, 1)$, computed while identifying the first-order kernel. A procedure for computing $\boldsymbol{h}_2(n, i)\, i = 1, 2, \ldots, n$, when all of the components of first-order kernel and the components $\boldsymbol{h}_2(i, j)\, i = 1, 2, \ldots, n-1;\ j = 1, 2, \ldots, n-1$ are known, is outlined next.

The excitation input vectors are defined as

$$u_k^{\mathrm{nl}}(i) = \bar{u}_0 \qquad \text{for} \qquad i \le k$$

$$u_k^{\mathrm{nl}}(i) = 2\bar{u}_0 \qquad \text{for} \qquad i > k \tag{29}$$

Define the Q terms containing only the nonlinear components of the response that are excited by the nth unknown vector as

$$Q_k(n) = \frac{P_k(n)}{\bar{u}_0^2} - 4\sum_{i=1}^{n-k}\sum_{j=1}^{n-1} h_2(i, j) - \sum_{i=n-k+1}^{n-1}\sum_{j=n-k+1}^{n-1} h_2(i, j) \tag{30}$$

where

$$Q_k(n) = f[P_k(n), h_2(i, j)], \qquad i, j = 1 \cdots n-1 \tag{31}$$

The equations for excitation u_{nl}^k become

$$2\sum_{i=1}^{n-k} h_2(n, i) + 2\sum_{i=1}^{n-1} h_2(n, i) + h_2(n, n) = Q_k(n) \qquad k = 1 \cdots n \tag{32}$$

The solution of the linear system of Eqs. (32) can be obtained as

$$h_2(n, n) = 2Q_n(n) - Q_1(n) \tag{33}$$

$$h_2(n, i) = [Q_{n-i}(n) - Q_{n-i+1}(n)]/2 \qquad \text{for} \qquad i = 1, 2, \ldots, n-1 \tag{34}$$

C. Approximate Convolution Procedures

Because the cost of identifying the second-order ROM kernels is high and the nonlinearity is weak, assuming that a reasonable prediction of the response can be obtained by executing only the first convolution is an option. This is an approximation to a more detailed solution. The predicted y_p and real responses are

$$y_p(n) = \sum_{i=1}^{n} h(n-i+1)u(i) \tag{35}$$

$$y(n) = \sum_{i=1}^{n} h_1(n-i+1)u(i) + \sum_{i=1}^{n}\sum_{j=1}^{n} \times h_2(n-i+1, n-j+1)u(i)u(j) \tag{36}$$

One option for computing h is to set $h = h_1$, where h_1 is the first-order Volterra kernel. This will provide a linearized response for a nonlinear system. The choice of the vector $\boldsymbol{h}$ has to provide exact predictions for linear systems and reasonable predictions for weakly nonlinear systems.

1. *Convolution of First-Order ROM Kernel*

The predicted response is

$$y_p(n) = \sum_{i=1}^{n} h_1(n-i+1)u(i) \tag{37}$$

For a linear system ($h_2 = 0$) the predicted response y_p is identical to the real response of the system. The associated error is

$$\Delta y_{h_2=0}(n) = y_{h_2=0}(n) - y_p(n) = \left[\sum_{i=1}^{n}\sum_{j=1}^{n} h_2(n-i+1, n-j+1)u(i)u(j)\right]_{h_2=0} = 0 \tag{38}$$

Thus, the approximate kernel h provides a good prediction of the response of the linearized system. However, for quadratic nonlinear systems ($h_2 \neq 0$) the error is

$$\Delta y(n) = y(n) - y_p(n) = \sum_{i=1}^{n}\sum_{j=1}^{n} h_2(n-i+1, n-j+1)u(i)u(j) \tag{39}$$

which is not equal to zero as a rule for an arbitrary excitation $u(i)$. The use of the preceding approximate kernel to predict the response of different quadratic nonlinear systems with different second-order ROM kernels is examined next.

Define the Jacobian of the function $y(h_1, h_2)$ as

$$J(i, j, k) = \frac{\partial y(i)}{\partial h_2(j, k)} \tag{40}$$

For the real response, J (third-order tensor) is

$$J(i, j, k) = [2 - \delta(j, k)]u(n-j+1)u(n-k+1) \tag{41}$$

where $\delta(j, k)$ is the Kronecker delta function. If $u(n-j+1)$ is not zero, then the Jacobian for the ith value of the predicted response is a full nonzero matrix. For the just-mentioned ROM kernel approximation,

$$J(i, j, k) = \frac{\partial y_p(i)}{\partial h_2(j, k)} = 0 \tag{42}$$

for any type of excitation. This means that the predicted response is the same for all systems with the same linear characteristics even if there are different quadratic kernels.

2. Basic Constraints

Three basic constraints are imposed on the computations of the kernels:

1) The predicted response has to be sensitive to nonlinear perturbations. That is, the Jacobian matrix of the predicted response as a function of the second-order kernel should not be zero and should contain a reasonable number of nonzero terms for nonzero inputs. (The optimal value for an n-size kernel is n^2.) $J[i]_{nxn}$ [Eq. (42)] should contain a reasonable number of nonzero terms for a quadratic nonlinear system.

2) The predicted response has to be accurate for linear systems. The linearized ROM kernel should be equal to the linear Volterra kernel for linear systems [$h_2(i, j) = 0$ for any i, j]:

$$[y_p(i)]_{h_2=0} = [y(i)]_{h_2=0} \tag{43}$$

3) The predicted response must be exact for the inputs that generated the kernels. This means that the difference between the real response and the predicted response should be zero for all excitations that generated the equations. This constraint provides the mathematical basis for generating the equations:

$$\Delta y_{h_2\neq 0}(i) = y_{h_2\neq 0}(i) - y_{p_{h_2\neq 0}}(i) = 0 \tag{44}$$

Choosing an approximate kernel equal to the first-order ROM kernel violates the last constraint. However, the error term, as shown in the next two sections, is a function of the ratio between the current value of arbitrary input and the amplitude of the excitation. For higher ratios the predicted response underestimates the real response, and for lower ratios the solution is overestimated. Silva[9] proved that accurate solutions could be obtained by convolving the first-order Volterra kernel. By enforcing this constraint, the system of equations for h can be easily defined by assembling the excitation vectors and the output vectors. Although the first linear kernel for linear systems provides accurate predictions, the predicted response will be insensitive to strong nonlinear changes in the system.

Two options for the candidate excitations are investigated: exciting the system with pulse input and exciting the system with step input.

3. Convolution of the Pulse Response

For a pulse input given as

$$u(1) = \bar{u}_0, \qquad u(i) = 0 \quad for \quad i = 1 \cdots n \tag{45}$$

only the term $h_2(n_2, n_2)$ will have a nonzero coefficient and it will be excited. The response of the system is

$$p(n) = \bar{u}_0 h_1(n) + \bar{u}_0^2 h_2(n, n) \tag{46}$$

Enforcing the preceding third constraint gives

$$p(n) = \bar{u}_0 h(n) \tag{47}$$

Solving the preceding equation leads to the vector to be convolved as

$$h(n) = p(n)/\bar{u}_0 \tag{48}$$

This vector is proportional to the pulse response of the system and is dependent on the amplitude of the pulse input. Expressing h in terms of h_1 and h_2,

$$h(i) = h_1(i) + \bar{u}_0 h_2(i, i) \tag{49}$$

The response predicted using the quasi-linear kernels would be

$$y_p(n) = \sum_{i=1}^{n} h_1(n - i + 1)u(i) + \sum_{i=1}^{n} h_2(n - i + 1, n - i + 1)\bar{u}_0 u(i) \tag{50}$$

For a linear system ($h_2 = 0$) this kernel will lead to an exact prediction of the response, thus satisfying the second constraint. The Jacobian can be expressed as

$$J_p(i, j, k) = \bar{u}_0 u(i)\delta(j, k) \tag{51}$$

4. Convolution of the Derivative of the Step Response

To improve the excitation of the quadratic kernel in the identification of the approximate kernel, $u(i)u(j)$ should be nonzero for any i and j, and the whole quadratic kernel would be excited. A step response excitation is proposed. It is

$$u(i) = \bar{u}_0 \qquad for \qquad i = 1 \cdots n$$

$$y(n) = \bar{u}_0 \sum_{i=1}^{n} h_1(n - i + 1) + \bar{u}_0^2 \sum_{i=1}^{n}\sum_{j=1}^{n} h_2(n - i + 1, n - j + 1) \tag{52}$$

The $y(n)$ response contains all quadratic terms $h(i, j)$. Imposing the third constraint leads to

$$y_s(n) = \bar{u}_0 \sum_{i=1}^{n} h(n - i + 1) \tag{53}$$

Defining the variation of the step response as

$$\Delta y_s(1) = y_s(1), \qquad \Delta y_s(i) = y_s(i) - y_s(i - 1) \quad for \quad i > 1 \tag{54}$$

the solution for the kernel is

$$h(n) = \Delta y_s(n)/\bar{u}_0 \tag{55}$$

The ROM kernel is proportional to the derivative of the step response of the system and is dependent on the amplitude of the pulse input. Expressing h in terms of h_1 and h_2 gives

$$h(i) = h_1(i) + 2\bar{u}_0 \sum_{k=1}^{n} h_2(i, n - k + 1) + \bar{u}_0 h_2(i, i) \tag{56}$$

The predicted response using the convolution of the derivative of the step response will be, for an arbitrary input $u(i)$,

$$y_s(n) = \sum_{i=1}^{n} h_1(n - i + 1)u(i) + \sum_{i=1}^{n} h_2(n - i, n - i)\bar{u}_0 u(i) + 2\sum_{i=1}^{n}\sum_{k=1}^{n-1} h_2(n - i + 1, n - k + 1)\bar{u}_0 u(i) \tag{57}$$

The Jacobian of the predicted response is now a fully nonzero matrix, leading to a better response using a kernel computed with this algorithm:

$$J_s(i, j, k) = [4 - \delta(j, k)]\bar{u}_0 u(i) \tag{58}$$

The response computed using the ROM kernel obtained from the step response contains all of the terms for the second-order kernel in an averaged way.

IV. Results and Discussion

A. ROM Results

1. First- and Second-Order Kernels for Ricatti Equation

The Ricatti equation was used in order to validate the identification algorithm for the first- and second-order ROM kernels. The first-order ROM kernel was computed by solving both the equations generated from step responses and pulse responses. The predicted response using the first three ROM kernels was compared with the

exact solution for a sinusoidal excitation. The equation integrated was

$$\frac{dy}{dt} + \alpha y + \varepsilon y^2 = x(t), \qquad \alpha = 0.01, \qquad \varepsilon = 0.0001 \quad (59)$$

The amplitude of step and pulse excitations was $1.0 \times 10,^{-15}$ and the time step used for the solution was $\Delta t = 1$. The solution obtained by convolving the first-order ROM kernel (Fig. 1) was accurate enough to justify the use of approximate convolution procedures (convolution of impulse response and the convolution of derivative of step response).

The identified first-order ROM kernels (Fig. 1) are the same, when computed from the step response as well as the pulse response. The averaged per time step L2 norm is 1.55×10^{-15}. The computational effort was almost the same as well between the two cases.

Figure 2 shows the second-order ROM kernel for the Ricatti equation. The kernel is diagonally dominant. This structure of the kernel explains the accurate results obtained using the convolution of the impulse response method, where only the diagonal terms of the second-order ROM kernel are included in the linearized kernel.

Figure 3 shows a comparison between the exact solution of Ricatti equation and the linear and quadratic ROM convolutions. The averaged per time step L2 norm is 0.026 for the linear convolution and 0.013 for the quadratic convolution. Both ROM models predicted responses approximate well the exact response, justifying the linear approximation of the model.

2. *Generalized Responses Using Reduced-Order-Modeling Approach*

To investigate the results obtained using approximate convolution procedures, the ROM kernels were identified for following three different methods: 1) convolution of the derivative of the step response (method 1); 2) convolution of the impulse response (method 2); and 3) convolution of the derivative of displacement with the step response (method 3). A NACA0012 typical section model is considered as an example. The CFD transient response is obtained by using the conventional approach (integrating the nonlinear Navier–Stokes equations). This response is used for the validation of the solutions predicted using the linearized ROM kernels with the procedures just described.

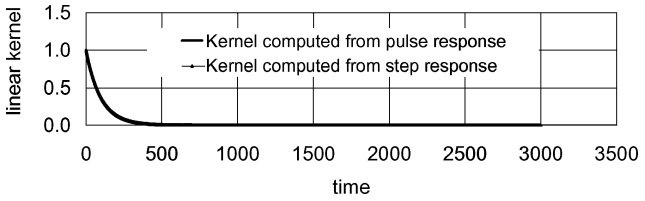

Fig. 1 First-order kernels for Ricatti equation.

Figure 4 shows the ROM kernels for methods 1 and 2. The kernels (the derivative of the step response for method 1 and the impulse response for method 2) have almost equal values, indicating the weakly nonlinear behavior of the aerodynamic system.

The aerodynamic responses caused by a Gaussian pulse applied on both modes (pitch and plunge) are determined using the preceding ROM methods and compared with the results obtained from conventional approach. For this comparison, a freestream Mach number of 0.62 and a dynamic pressure of 120 psf are used. A small nondimensional time step of 0.002 (4.25×10^{-6} s) was used for the integration of the Navier–Stokes equations. The equation of the simultaneously applied Gaussian pulse is $h = \alpha = 0.05e^{-0.95(\tau - 3)^2}$. The inputs applied on both modes are shown in Fig. 5.

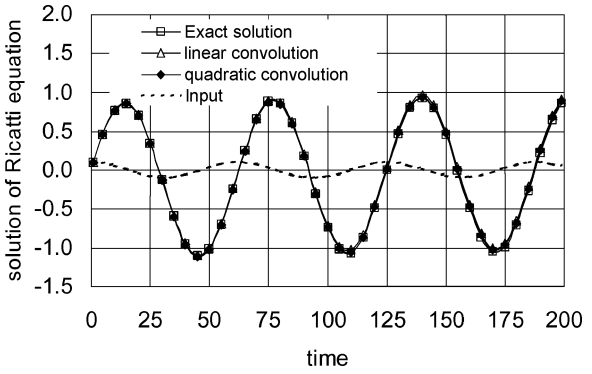

Fig. 3 Comparison of solutions of Ricatti equation for sinusoidal excitation.

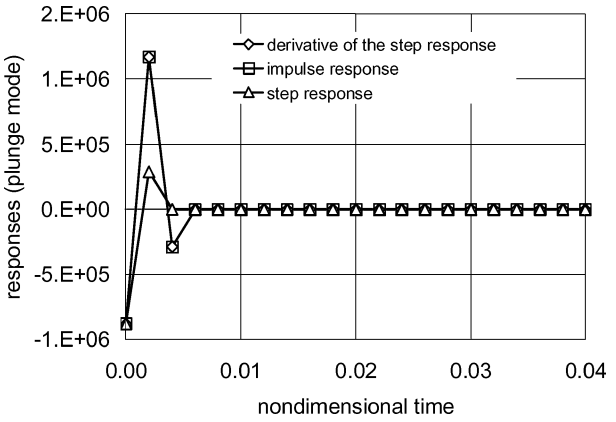

Fig. 4 Step/impulse responses of typical section model: $M = 0.62$ and $q = 120$ psf.

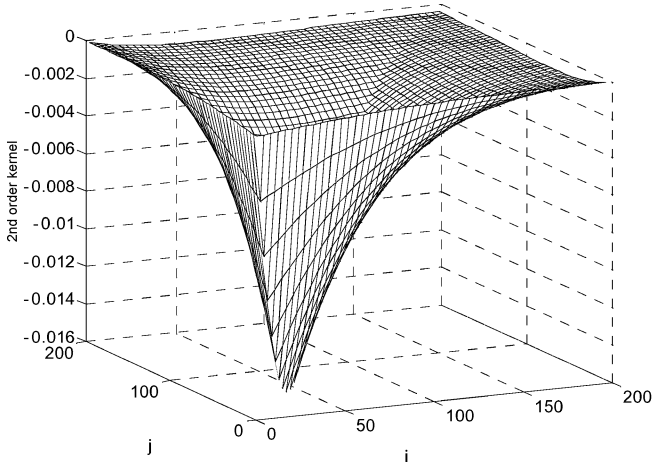

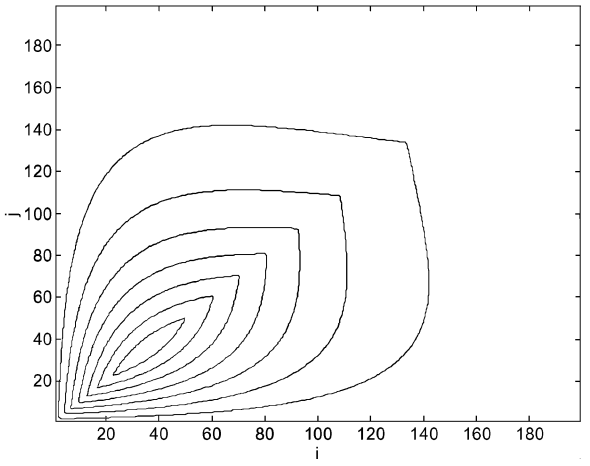

Fig. 2 Second-order ROM kernel computed from step excitation.

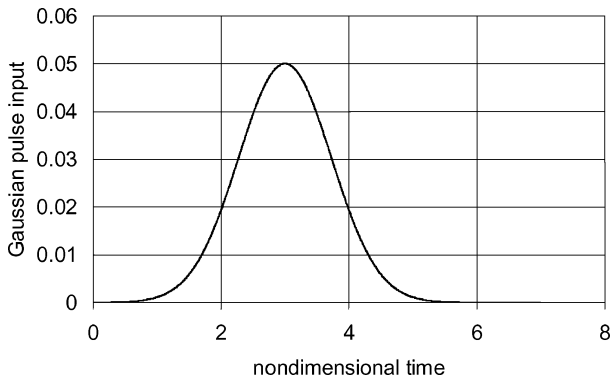

Fig. 5 Gaussian pulse inputs for typical section model.

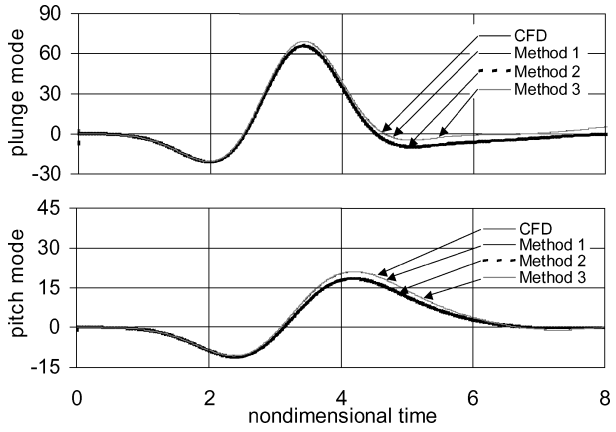

Fig. 6 Generalized forces caused by Gaussian pulse input: $M = 0.62$ and $q = 120$ psf.

Figure 6 shows the accurate results for methods 1 and 2, and approximate solution for method 3. The two more accurate methods are based on step response, whereas the least accurate identifies the linearized kernels using the impulse response of the aerodynamic system. The averaged per time step L2 norm of the prediction error for the plunge mode is 0.069 and 0.094 for method 1 and method 3, respectively, and 3.212 for method 2. The same trend is present on the values of the average L2 norm for the pitch mode where the averaged per time step L2 norm for method 2 is 0.954 and at least one order of magnitude for the method 1 and method 3, 0.003 and 0.035, respectively.

The difference between method 1 (convolution of the derivative of the step response) and method 2 (convolution of the impulse response) can be explained in two ways. One of them is related to the proper identification of the impulse response. The CFD solver is expected to provide more accurate responses when excited with a step input rather than the pulse input because of the lower gradients. The second reason is related to the way the two ROM methods include the aerodynamic nonlinearities. A measure of how well the nonlinear effect is included in the transient response is the Jacobian [Eq. (40)]. The Jacobian of the method 1 response approximates that of the real response better than the Jacobian of method 2. Although the Jacobian of the real response is a full nonzero matrix, the Jacobian of the impulse response is only a diagonal matrix. Based on these results, further investigations for ROM will be developed using the convolution of the derivative of the step response.

To validate the use of the ROM kernel for a wide range of Mach numbers, a set of CFD and method 1 computations were carried out (Fig. 7). The ROM kernel was convolved to predict the aerodynamic response for the Gaussian pulse.

The prediction of the Gaussian pulse response using the convolution of the derivative of the step response is very accurate. A comparison of the predicted transient response (using method 1, the derivative of the step response) with the transient response obtained using the conventional approach at different Mach numbers

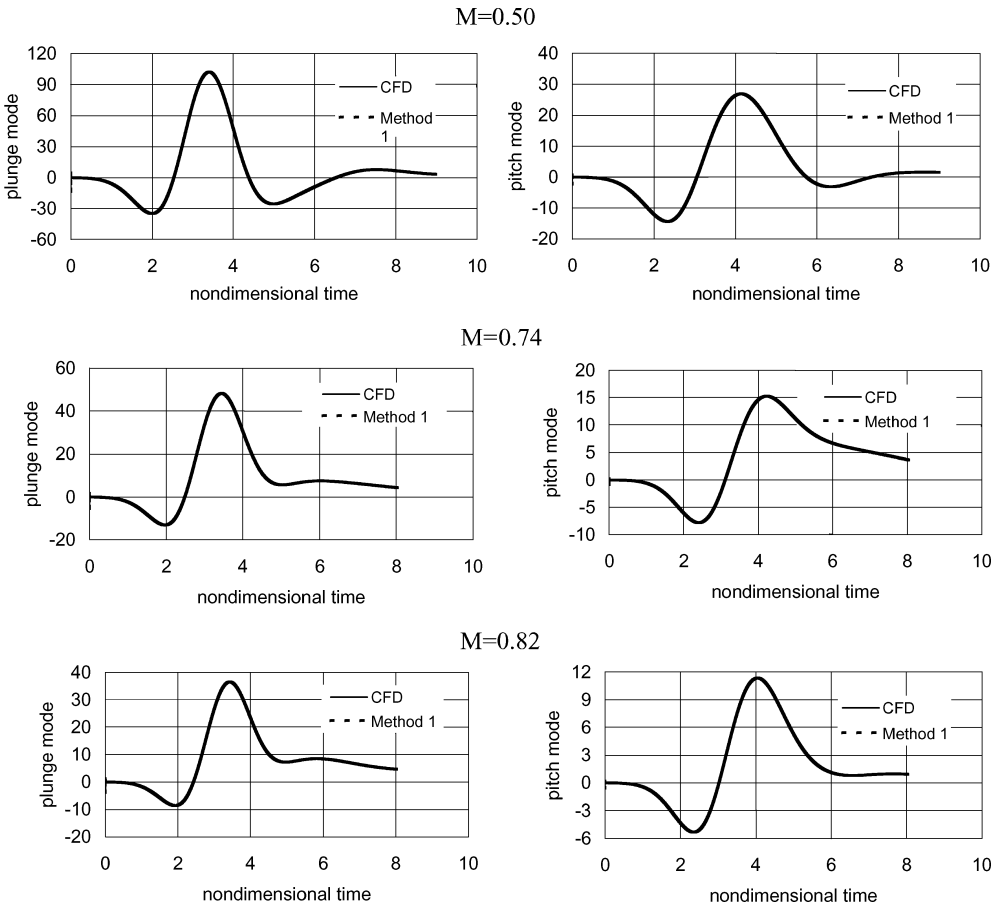

Fig. 7 Generalized force caused by a Gaussian pulse: $q = 120$ psf.

is presented in Fig. 7. The average per time step L2 norms of the prediction error are 0.089 for the plunge mode and 0.028 for the pitch mode at $M = 0.5$. The same accuracy is obtained for the transonic regime: at $M = 0.82$ the averaged per time step L2 norms are 0.042 and 0.016 on the plunge and pitch mode, respectively.

To investigate the appropriate time step to be used for the identification of the ROM kernel, a set of CFD and method 1 computations was also done using a relatively coarse time step ($dt = 0.1$). The predicted responses obtained using the large time step were compared with the ones computed using the conventional approach, and they were the same (Fig. 8). This shows that the step response provides robust ROM kernels for a large range of time steps.

The predicted response obtained by using the convolution of the derivative of the step response (method 1) has the same accuracy as the predicted responses using the small time step. The averaged per time step L2 norms of the prediction error are 0.065 for the plunge mode and 0.031 for the plunge mode.

B. Nonlinear Aeroelastic Analysis Results

1. Structural and Aerodynamic Models

A two-degree-of-freedom typical section model is used to investigate structural nonlinear effects on aeroelastic responses along with existing aerodynamic nonlinearity.[22] To see the structural nonlinearity effects, the following three different models were considered.

1) Linear model:

$$\sigma_\alpha = \sigma_{\alpha l}, \qquad \sigma_h = \sigma_{\mathrm{hl}}$$

2) Nonlinear model that has a higher-order term in pitch direction:

$$\sigma_\alpha = \sigma_{\alpha l} + \sigma_{\alpha \mathrm{nl}}\alpha^2, \qquad \sigma_h = \sigma_{\mathrm{hl}}$$

3) Free-play model in both plunge and pith directions:

$$\sigma_\alpha = \sigma_{\alpha l}\delta(\alpha_0) - \sigma_{\alpha l}\delta(-\alpha_0), \qquad \sigma_h = \sigma_{\mathrm{hl}}\delta(h_0) - \sigma_{\mathrm{hl}}\delta(-h_0)$$

where $\sigma_{\alpha l}$ is the effective stiffness on the pitch mode in the linear model, $\sigma_{\alpha \mathrm{nl}}$ is the quadratic term in the pitch-hardening effective stiffness, and δ is the step function. These models are solved with the algorithm just presented.

Figure 9 shows the aerodynamic grid (177/65) of the NACA 0012 airfoil used for flowfield evaluations here. The Spalart–Almaras turbulence model used was for the computations. The sea level density of the fluid is is 81.84 lb/ft^3(R-12 gas). A schematic of the structural model is shown in Fig. 10. Some of the important parameters of the wing are presented in Table 1.

Table 1 Structural parameters

Parameter	Value
Mass	6.08 slug
Chord	16 in.
Pitch inertia	2.8 slug · ft^2
Pitch stiffness	3000 lb-ft
Plunge stiffness	2686 lb/ft
Plunge frequency	21.01 rad/s
Pitch frequency	32.72 rad/s
Damping ratio: plunge	0.0014
Damping ratio: pitch	0.001
Plunge free play/chord	3.2×10^{-4}
Pitch free play	1.8×10^{-3} deg
Plunge free play/chord	4.8×10^{-4}
Pitch free play initial perturbation	2.7×10^{-3} deg
Nonlinear pitch stiffness $\sigma_{\alpha \mathrm{nl}}$	8.74×10^6 lb-ft

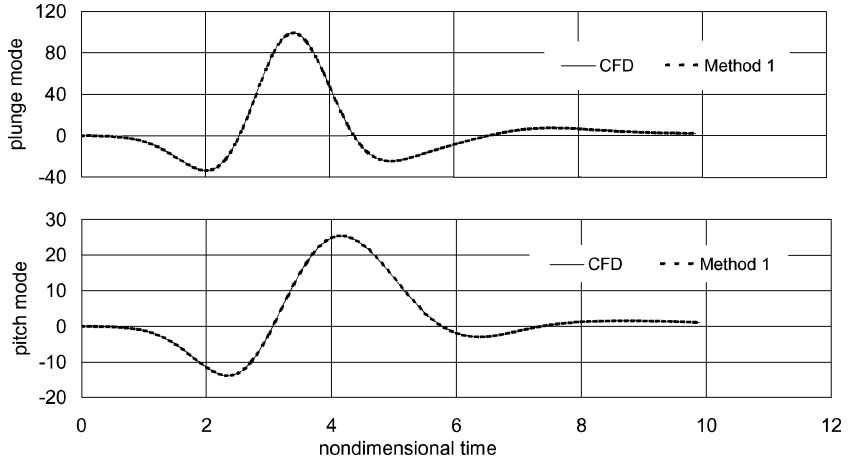

Fig. 8 Generalized forces for a Gaussian pulse for $M = 0.50$, $q = 120$ psf, and $\Delta t = 0.1$.

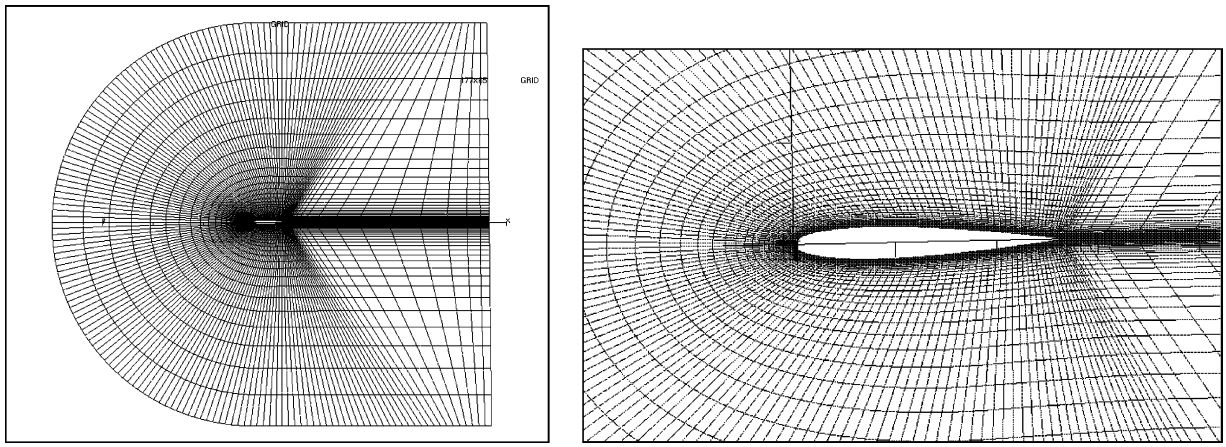

Fig. 9 Aerodynamic grid of NACA 0012 airfoil.

2. Transient Response Comparison

The generalized responses of the aeroelastic system were computed for a range of Mach numbers between $M = 0.52$ and 0.82. The aeroelastic responses computed using the convolution of the derivative of the step response were compared with the results obtained from the CFL3D computations for the linear, quadratic nonlinear, and a free-play structural model. The convolution of the derivative of the step response provided accurate predictions of the aerodynamic response to an arbitrary input. Although the identification of the kernels is less efficient computationally, it is robust and provides accurate results for a wide range of step amplitudes and time steps. For smaller time steps, the results are extremely accurate (below 1%), whereas for large time steps ($dt = 0.1$) the flutter dynamic pressures are predicted with an accuracy of about 2%. The ROM kernel for the convolution of the derivative of the step response provides a full average of the second-order kernel, including all nonlinear terms. The nonlinear approximation is accurate for arbitrary inputs with amplitudes in the range of the step input amplitudes that generated the ROM kernel. The Jacobian of the predicted response is a full nonzero matrix and better approximates the Jacobian of the real response when the step excitations and arbitrary input have the same order of magnitude. Figures 11–14 show representative results of the computations.

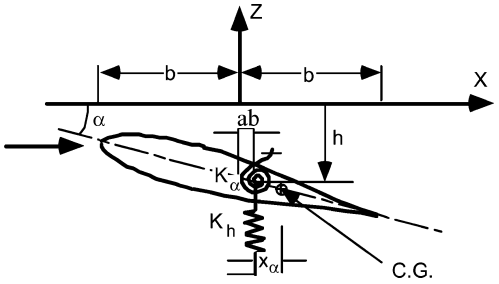

Fig. 10 Schematic of the two-dimensional typical section model.

The transient response predicted using the ROM approach approximates very well the responses obtained using the conventional approach. Figure 11 shows a comparison of the flutter prediction using the ROM and conventional approach. The flutter dynamic pressure was approximated with an error of 1.2%. At $M = 0.62$ accurate responses where obtained for transient responses having

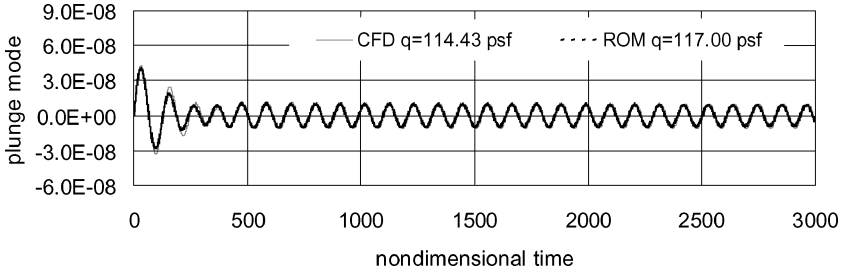

Fig. 11 Transient results for CFL3D and method 1 for $M = 0.50$ and $\Delta t = 0.1$: linear model.

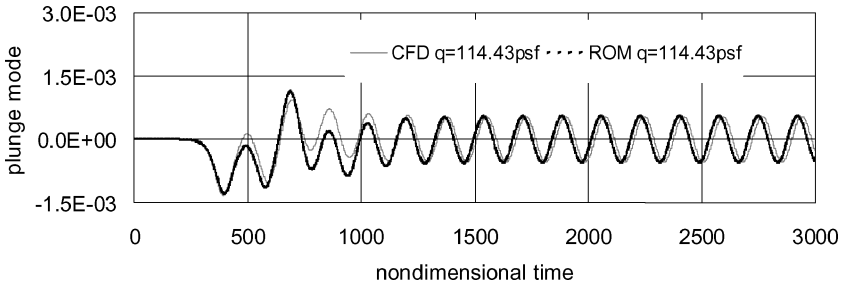

Fig. 12 Transient results for $M = 0.5$ and $\Delta t = 0.1$: free-play model.

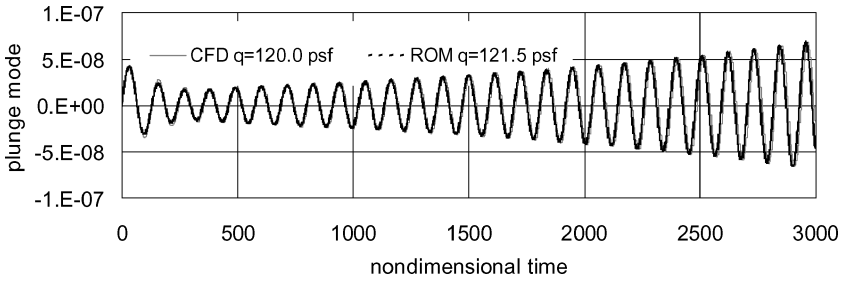

Fig. 13 Transient results for $M = 0.62$ and $\Delta t = 0.1$: linear model.

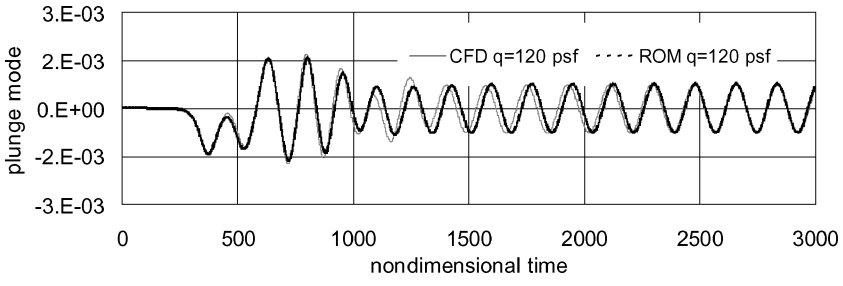

Fig. 14 Transient results for $M = 0.62$ and $\Delta t = 0.1$: free-play model.

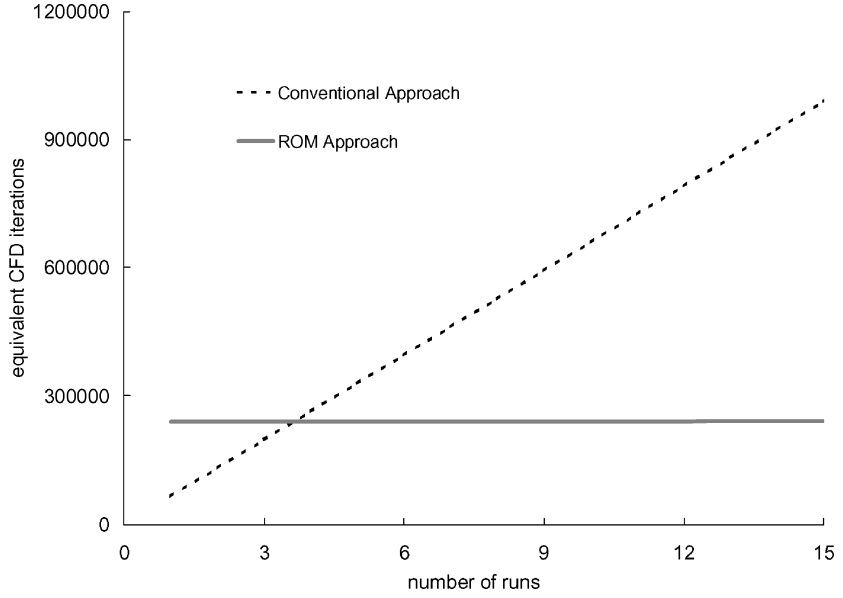

Fig. 15 Comparison of the cost using the conventional and the ROM approach.

Table 2 Computational time comparison

Conventional approach	ROM approach
Steady-state solution: total 6000 subiterations	ROM kernel identification: total 240,000 subiterations. (=2 modes × 3,000 iterations × 40 subiterations/iteration)
Dynamic solution: total 60,000 subiterations (=30,000 iterations × 2 subiterations/iteration)	Integration of aeroelastic equation: 30 equivalent CFL3D subiterations/case
Total cost: 66,000 × N cases	Total cost: 240,000 + 30 × N cases

different order of magnitude (Figs. 13 and 14). The transient response has larger errors after the initial perturbation (Fig. 12), but the responses from ROM approach can predict frequency and amplitude of the conventional approach response. The results suggest that the method is suitable to be used for the flutter and limit-cycle oscillations analysis.

3. Computational (CPU) Time Comparison

To estimate the increase in speed using the ROM approach, the computation cost in equivalent CFL3D subiterations was estimated. The computational effort to integrate one ROM iteration (integration of one time step) is about 0.1% of the cost to integrate one CFL3D subiteration. The estimation is made for a set of runs needed for computing the flutter dynamic pressure for a specific Mach number. For the CFL3D approach, the cost is proportional to the number of runs, whereas for the ROM approach there is an initial cost of the kernel identification for all of the runs, which is added to a small computational cost per each run. A coarse time step ($dt = 0.1$) was used for building the ROM kernel, and the results were compared with full CFD computations. The number of subiterations used in CFL3D computations is detailed on Table 2. Figure 15 shows the computational cost comparison between the two approaches.

The ROM approach is suited for flutter dynamic pressure investigations, where several computations have to be made to find the flutter envelope and the lower and upper bound of dynamic pressures where the limit-cycle oscillations occur. In the conventional approach the integration of Eq. (18) contains two integration steps for estimation of generalized coordinates and only one for the flowfield, whereas in the ROM approach because of the inexpensive cost of prediction of the next step generalized force three estimations of the generalized aerodynamic force are computed per time step.

An explanation for the computational efficiency of the ROM compared to the conventional approach is that the aerodynamic ROM generates only the flowfield information relevant to the aeroelastic problem unlike the conventional approach, which generates the

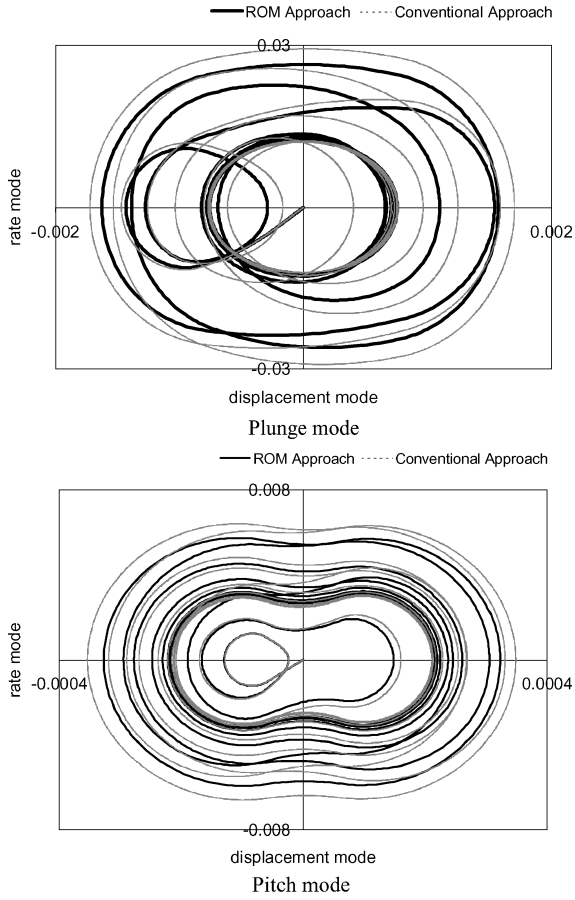

Fig. 16 Phase diagram for plunge and pitch modes at $M = 0.62$ and $q = 120$ psf.

complete the flowfield every time, thus using a large amount of computational resources. The identification procedure for the ROM model is input output based on the aeroelastic interface defined by the generalized aerodynamic forces and generalized displacements. The nature of the identification produces ROM that do not include the states that are unobservable or uncontrollable through the aeroelastic interface, thus reducing significantly the required computational memory and increasing the computational speed. The ROM contains only the states that are affected through the aeroelastic interface, thus providing accurate nonlinear aeroelastic response.

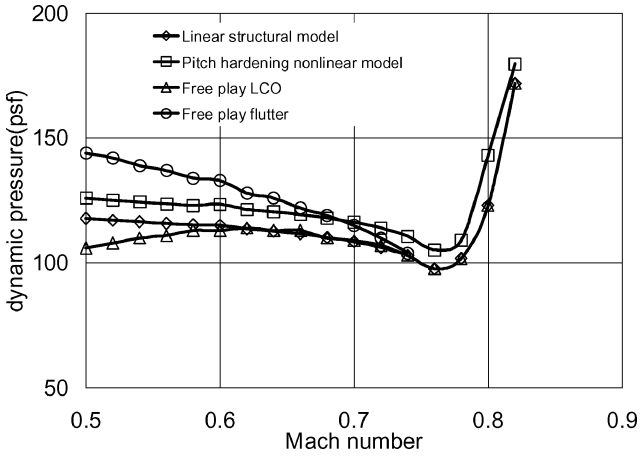

Fig. 17 Flutter dynamic pressure vs Mach number, method 1, $\Delta t = 0.1$.

4. LCO and Flutter Speed vs Mach Number

LCO analysis was conducted for the free-play nonlinear structural model using method 1 (Fig. 16).

The phase diagrams shown in Fig. 16 show accurate prediction of generalized forces while the chaotic motion is present. The results suggest that the ROM approach can be used for structural models with different types of nonlinearities without loss of accuracy.

Figure 17 shows the flutter envelope computed using the convolution of the derivative of the step response. The ROM model is able to capture the limited-cycle oscillations range, as well as the transonic dip at about Mach 0.77, in the transonic region. The presence of structural nonlinearities generated higher flutter dynamic pressures and a region of LCO in the transient response. The impact of structural nonlinearities is more significant in the subsonic region where the aerodynamic nonlinearities are not dominant. The preceding results indicate that the ROM approach is able to accurately estimate the LCO phenomenon.

V. Conclusions

The development of a methodology for using the reduced-order-model (ROM) technology for the nonlinear aeroelastic analysis has been presented along with representative results obtained using the method. A procedure for identifying the first- and second-order ROM kernels was presented. The method was applied first to a nonlinear problem described by the Ricatti equation, where the first- and second-order Volterra kernels were identified. Three different ROM approaches (convolution of the impulse response, convolution of the step response, and convolution of the derivative of the step response) were presented and compared. Gaussian pulse responses were calculated based on the proposed three methods and compared with the full computational-fluid-dynamics (CFD) (conventional approach) results for validation. The results show that the approach using convolution of the derivative of the step response gives better accuracy because the approximated response averages the effect of the full second-order Volterra kernel. The nature of the structural nonlinearities (free-play and pitch hardening) do not affect the linearized modal shapes during the time integration. The flutter envelope was built using the ROM approach, and the transonic dip was identified. The limit-cycle oscillations generated by the structural nonlinearities are accurately identified the ROM. The ROM approach is computationally efficient compared with the conventional approach and is well suited for addressing the aeroelastic problem in a computationally efficient manner. The increase in the computational speed using the ROMs was of about 1000 times compared to the conventional CFD approach. The convolution of the derivative of the step response method captures in an averaged way the nonlinear nature of the aerodynamic system, providing more accurate response than the convolution of the impulse response. Efforts are underway on developing procedures to identify higher-order ROM models including stronger nonlinearities for three-dimensional aeroelastic problems including the issue of nonlinear structural modal shapes.

Acknowledgment

The authors acknowledge the technical and financial support received from NASA Langley Research Center, Hampton, Virginia. The Technical Monitor was Walter Silva.

References

[1]Weisshaar, T. A., Nam, C., and Batista-Rodriguez, A., "Aeroelastic Tailoring for Improved UAV Performance," AIAA Paper 98-1757, April 1998.

[2]Smith, M. J., Patil, M. J., and Hodges, D. H., "CFD-Based Analysis of Nonlinear Aeroelastic Behavior of High-Aspect Ratio Wings," AIAA Paper 2001-1582, April 2001.

[3]Park, K. C., Felippa, C. A., and Ohayon, R., "Partitioned Formulation of Internal Fluid-Structure Interaction Problems by Localized Lagrange Multipliers," *Computer Methods in Applied Mechanics and Engineering*, Vol. 190, 2001, pp. 2989–3007.

[4]Beckert, A., "Coupling Fluid (CFD) and Structural (FE) Models Using Finite Interpolation Elements," *Aerospace Science Technology*, Vol. 4, No. 1, 2000, pp. 13–23.

[5]Rajadas, J. N., Chattopadhyay, A., and Pagaldipti, N., "Multidisciplinary Optimization Procedure for High Speed Aircraft Using Semi-Analytical Sensitivity Analysis Procedure and Multilevel Decomposition," *Engineering Optimization*, Vol. 31, 1998, pp. 25–51.

[6]Talya, S., Rajadas, J. N., and Chattopadhyay, A., "Multidisciplinary Design Optimization of Film-Cooled Gas Turbine Blades," *Mathematical Problems in Engineering*, Vol. 5, No. 2, 1999, pp. 97–119.

[7]Felippa, C. A., Park, K. C., and Farhat, C., "Partitioned Analysis of Coupled Mechanical Systems," *Computer Methods in Applied Mechanics and Engineering*, Vol. 190, 2001, pp. 3247–3270.

[8]Farhat, A., and Lesoinne, M., "Higher-Order Staggered and Subiteration Free Algorithms for Coupled Dynamic Aeroelasticity Problems," AIAA Paper 98-0516, Jan. 1998.

[9]Silva, W. A., "Identification of Linear and Nonlinear Aerodynamic Impulse Responses Using Digital Filter Techniques," AIAA Paper 97-3712, Aug. 1997.

[10]Lee-Rausch, E. M., and Batina, J. T., "Wing Flutter Computations Using an Aerodynamic Model Based on the Navier–Stokes Equations," *Journal of Aircraft*, Vol 33, No. 6, 1996, pp. 1139–1148.

[11]Tang, L., Bartels, R. E., Chen, P. C., and Liu, D. D., "Simulation of Transonic Limit Cycle Oscillations Using a CFD Time-Marching Method," AIAA Paper 2001-1290, April 2001.

[12]Hall, K. E., Thomas, J. P., and Dowell, E. H., "Reduced-Order Modeling of Unsteady Small Disturbance Flows Using a Frequency-Domain Proper Orthogonal Decomposition Technique," AIAA Paper 99-0655, Jan. 1999.

[13]Ko, J., Strganac, T. W., and Kurdila, A. J., "Adaptive Feedback Linearization for the Control of a Typical Wing Section with Structural Nonlinearities," *Nonlinear Dynamics*, Vol. 18, No. 3, 1999, pp. 298–301.

[14]Dowell, E., Edwards, J., and Strganac, T., "Nonlinear Aeroelasticity," *Journal of Aircraft*, Vol. 40, No. 5, 2003, pp. 857–874.

[15]Thomas, J. T., Hall, K. C., and Dowell, E. H., "Reduced-Order Aeroelastic Modeling Using Proper-Orthogonal Decompositions," CEAS/AIAA/ICASE/NASA Langley International Forum on Aeroelasticity and Structural Dynamics 1999, Williamsburg, VA, June 1999.

[16]LeGresley, P. A., and Alonso, J. J., "Investigation of Non-Linear Projection for POD Based Reduced Order Models for Aerodynamics," AIAA Paper 2001-0926, Jan. 2001.

[17]Silva, W. A., "Reduced Order Models Based on Linear and Nonlinear Aerodynamic Impulse Response," AIAA Paper 99-1262, April 1999.

[18]Raveh, D. E., Levy, Y., and Karpel, M., "Aircraft Aeroelastic Analysis and Design Using CFD-Based Unsteady Loads," AIAA Paper 2000-1325, April 2000.

[19]Silva, W. A., and Raveh, D. E., "Development of Unsteady Aerodynamic State-Space Models from CFD-Based Pulse Responses," AIAA Paper 2001-1213, April 2001.

[20]Silva, W. A., and Bartels, R. E., "Development of Reduced-Order Models for Aeroelastic Analysis and Flutter Prediction Using the CFL3Dv6.0 Code," AIAA Paper 2002-1596, April 2002.

[21]Lucia, D. J., Beran, P. S., and Silva, W. A., "Aeroelastic System Development Using Proper Orthogonal Decomposition and Volterra Theory," AIAA Paper 2003-1922, April 2003.

[22]Munteanu, S., Rajadas, J., Nam, C., and Chattopadhyay, A., "A Quasi-Linear Approach for Solving Aeroelastic Problems Involving Aerodynamic and Structural Nonlinearities," AIAA Paper 2003-1401, April 2003.

[23]Cunningham, H. J., Batina, J. T., and Bennet, R. M., "Modern Wing Flutter Analysis by Computational Fluid Dynamics Methods," NASA TM 100531, Jan. 1988.

A. Palazotto
Associate Editor